JACS
JOURNAL OF THE AMERICAN CHEMICAL SOCIETY
Article
pubs.acs.org/JACS

Relationship between Interchain Interaction, Exciton Delocalization, and Charge Separation in Low-Bandgap Copolymer Blends

Zhi Guo,[†,‡] Doyun Lee,[§] Richard D. Schaller,[∥,#] Xiaobing Zuo,[⊥] Byeongdu Lee,[⊥] TengFei Luo,[‡] Haifeng Gao,[§] and Libai Huang*[,†]

[†]Radiation Laboratory, [‡]Department of Aerospace and Mechanical Engineering, and [§]Department of Chemistry and Biochemistry, University of Notre Dame, Notre Dame, Indiana 46556, United States

[∥]Center for Nanoscale Materials and [⊥]X-ray Science Division, Advanced Photon Source, Argonne National Laboratory, Argonne, Illinois 60439, United States

[#]Department of Chemistry, Northwestern University, Evanston, Illinois 60208, United States

Supporting Information

ABSTRACT: We present a systematic study of the roles of crystallinity, interchain interaction, and exciton delocalization on ultrafast charge separation pathways in donor−acceptor copoloymer blends. We characterize the energy levels, excited state structures, and dynamics of the interchain species by combined ultrafast spectroscopy and computational quantum chemistry approaches. The alkyl side chain of a highly efficient donor−acceptor copolymer for solar cell applications, PBDTTT (poly(4,8-bis-alkyloxybenzo-[1,2-b:4,5-b′]dithiophene-2,6-diyl-*alt*-(alkylthieno[3,4-*b*]thiophene-2-carboxylate)-2,6-diyl), is varied to tune the molecular packing and interchain interaction of the polymers in order to elucidate the charge separation pathways originating from intrachain and interchain species. Polymers with linear side chains result in more crystalline polymer domain that lead to preferential formation of interchain excitons delocalizing over more than one polymer backbone in the solid state. Our results demonstrate that the higher polymer crystallinity leads to slower charge separation due to coarser phase segregation and formation of the interchain excited states that are energetically unfavorable for charge separation. Such energetics of the interchain excitons in low-bandgap copolymers calls for optimized solar cell morphologies that are fundamentally different from those based on homopolymers such as P3HT (poly-3-hexylthiophene). A long-range crystalline polymer domain is detrimental rather than beneficial to solar cell performance for a low-bandgap copolymer which is in direct contrast to the observed behavior in P3HT based devices.

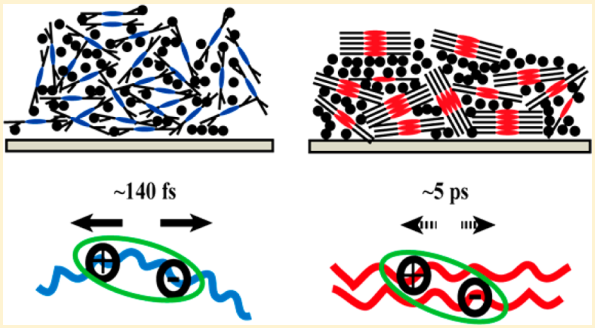

I. INTRODUCTION

In polymer-based bulk heterojunctions (BHJs), where conjugated polymer donor and fullerene based acceptor are intimately mixed to form interconnected micro- and nanoscale domains in a thin film, efficient conversion of solar energy to electricity requires a complex interplay between functional components and light harvesting and conversion processes occurring over a wide range of length and time scales.[1] Morphology, including the packing of the molecules and phase segregation of different compositions, plays a critical role in charge separation and transport processes.[2−10] Of particular importance is the molecular arrangement of the polymer and fullerene at the interface that determines the nature of the excited states and charge separation mechanism.[11−18] Why the photogenerated charge pairs are separated at a time scale of less than 100 fs despite the presence of the strongly bound exciton with a large Coulombic interaction energy is currently under debate. Several mechanisms have been invoked including vibrationally hot charge transfer states[14,19,20] and charge delocalization over extended domains.[15−18,21,22]

There are two types of excitons in conjugated polymers: along the chain (intrachain) or between chains (interchain). The intrachain excitons are typical Frenkel excitons; in other words, the collective excited states are linear combinations of electronic excitations of each chromophore within the conjugated unit.[23−28] The interchain excitons are interchain excited state species where electron density is shared between chromophores on neighboring polymer chains. When two polymer chromophores on adjacent chains share their π-electrons equally in the excited state but not in the ground state, the interchain excited state is called an "excimer".[29−33] In contrast, when π-electrons are neutrally delocalized over multiple segments in both the ground and excited states are known as "aggregates".[24,26,34] In addition to neutral electron

Received: April 7, 2014
Published: June 23, 2014

 © 2014 American Chemical Society dx.doi.org/10.1021/ja503465s | J. Am. Chem. Soc. 2014, 136, 10024−10032

delocalization between chains, charge transfer can occur upon excitation of strongly interacting chromophores, leading to charge-separated interchain species referred to as a "polaron pair".

The exact nature of excitons created by photoexcitation in conjugated polymers depends strongly on the polymer morphology because different molecular packing results in a dispersive distribution of exciton energies contributed by various intra- and interchain configurations.[23,24,26,30,35−40] One main challenge in unraveling the fundamental photophysical properties of conjugated polymers lies in the complex microstructures in the solid state resulting from the many degrees of conformational freedom. Ultrafast formation of interchain excitons with relatively high yield has been found in conjugated homopolymers such as MEH-PPV and P3HT.[29,37,41] Spectroscopic signatures of intrachain and interchain species have been investigated extensively in homopolymers by single molecule spectroscopy experiments.[40,42−44]

Recent improvement in OPV efficiency, with values now approaching 10%, was enabled through the use of low-bandgap copolymers employing donor−acceptor (or "push−pull") moieties along the polymer backbone such as seen in the PCDTBT(poly *N*-9′-heptadecanyl-2,7-carbazole-*alt*-5,5-4,7-di-2-thienyl-2′,1′,3′-benzothiadiazole), PBDTTT, and PTB (poly thienothiophene-benzodithiophene) families.[45−49] One important distinction in this group of polymers is that the lowest-energy excitonic transition exhibits partial charge-transfer character.[20,22,27,50−55] These intramolecular charge transfer states are proposed to facilitate final charge separation at the heterojunctions.[20,22,50−52,56]

Despite the success of this low-bandgap approach, understanding the photoexcitation pathways of this new group of polymers is still far from complete. In particular, how interchain interaction and exciton delocalization affect the primary photoexcited states and the consequent charge separation and transport pathways is unclear. Recent studies suggest that charge and exciton delocalization in both the polymer donors and the fullerene acceptors are critical for achieving ultrafast charge separation.[15,16,18,19] Ultrafast spectroscopy measurements on donor−acceptor copolymers have so far been focused on intrachain excited states.[20,22,27,50−53] Understanding the interchain interactions in relation to molecular packing is important because they are widely prevalent in solid state films and are critical factors for optimal charge separation. Morphology and crystallinity of the polymer domains are also important for optimizing charge transport.[8,9,57]

In this article, we systematically address how interchain interaction modulates charge separation and recombination dynamics in a highly efficient BHJ blend composed of low-bandgap copolymer PBDTTT series (the structure of the polymers is shown in Figure 1) and a fullerene acceptor (Phenyl-C61-butyric acid methyl ester, PCBM). We varied the alkyl side chains on the polymers to control the molecular packing and interchain interaction. Our results demonstrate that unlike solar cells based on P3HT, for low-bandgap copolymer such as PBDTTT, a crystalline polymer domain is detrimental instead of being beneficial to device performance.

II. RESULTS AND DISCUSSION

II.1. Structure Characterization of Neat Polymer Films and Bulk Heterojunctions. The alkyl side chains of the PBDTTT polymers were designed to systematically tune the crystallinity, with the linear side chains leading to higher crystallinity.[58] More details on the polymer synthesis can be found in our prior work.[59] p-Type low-bandgap conjugated copolymers poly(4,8-bis-alkyloxybenzo[1,2-*b*:4,5-*b*′]-dithiophene-2,6-diyl-*alt*-(alkylthieno[3,4-*b*]thiophene-2-carboxylate)-2,6-diyl (PBDTTT, Figure 1) were synthesized based on modified literature procedure.[60] The PBDTTT polymers are decorated with two alkyl groups on the three substitution sites. The alkyl side chain groups on the R1 and R2 positions include two groups: (1) ethyhexyl groups (branched structure, denoted as E) that provides solubility and processability for the polymers and (2) dodecyl groups (linear structure, denoted as D) that can enable high crystallinity. Four different combinations of substituted polymers on a PBDTTT backbone are available: PBDTTT-*EE*, PBDTTT-*ED*, PBDTTT-*DE*, and PBDTTT-*DD*, in which the first italic letter represents the species of the two identical substituted groups on the BDT unit and the second letter represents the substituted groups on the TT unit as shown in Figure 1. In both neat polymers films and BHJs, linear side chain leads to tighter $\pi-\pi$ stacking and stronger interchain interaction. Compared to linear alkyl chains, branched alkyl chains prevent interchain packing and results in weaker coplanar backbone interaction because of their bulkiness and the steric hindrance effects.[58] As a result, the crystallinity of the polymer films is expected to be in the following order: *DD* > *DE* > *ED* > *EE*.

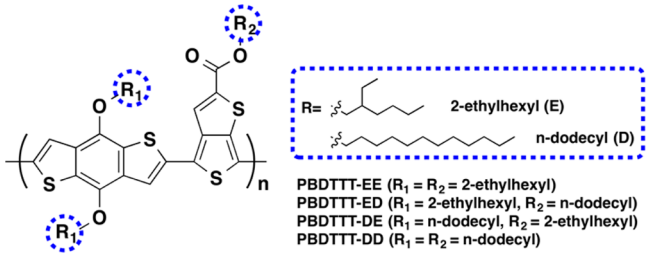

Figure 1. Molecular structures of PBDTTT polymers. The BDT unit is connected to two symmetric R_1 substitution sites, and the TT unit is connected to the R_2 substitution site. Four polymers are composed of different alkyl side chain substituion combinations using either 2-ethylhexyl or *n*-dodecyl.

We employed gazing incident small-angle X-ray scattering (GISAXS) and atomic force microscopy (AFM) imaging to investigate the structure and morphology of the BHJ films, with the experimental details presented in the Supporting Information (SI). As shown in the AFM images in SI Figure S1, the length scale of phase segregation differs significantly depending on the side chain structures, with finer phase segregation found in BHJs comprising polymers decorated with more branched side chains. The mix domain size of different BHJs revealed by AFM increases in the following order: *EE* (15−30 nm), *ED* (50−100 nm), *DE*(150−250 nm), and *DD* (300−500 nm). We note here that these domains in the AFM are not pure and consist of different sizes of nanocrystalline aggregates as discussed below.

The GISAXS experiments provide molecular-level structural information on polymer packing in the BHJs. The scattering patterns of the neat polymer films (SI Figure S2) revealed a parallel-to-substrate preference of the polymer backbone orientation. Figure 2 shows the scattering patterns of BHJs made from PBDTTT-*EE* and -*DD*. For each polymer, BHJs with varied loading of PCBM (33%, 50%, and 67%) and the corresponding neat films. The GISAXS pattern of the BHJs

dx.doi.org/10.1021/ja503465s | J. Am. Chem. Soc. 2014, 136, 10024−10032

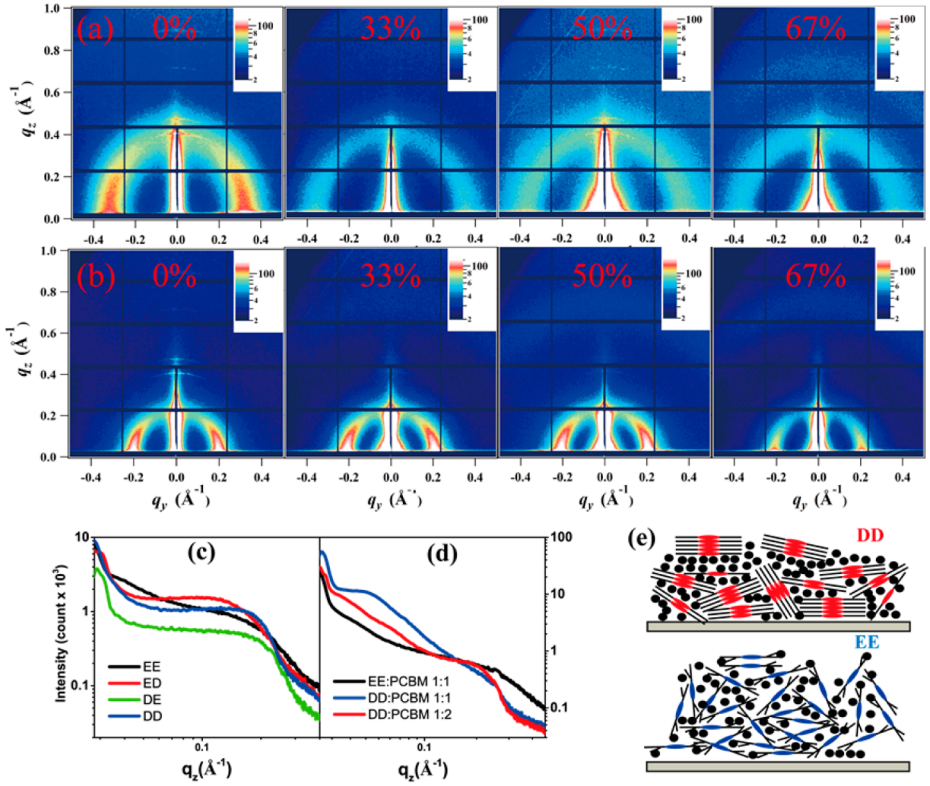

Figure 2. GISAXS patterns of two BHJs with different PCBM weight ratios (0%, 33%, 50%, 67%). (a) PBDTTT-*EE*:PCBM; (b) PBDTTT-*DD*:PCBM; (c,d) normal-to-plane line cut chosen at small in-plane scattering angle (q_y = 0.005 Å^{-1}), (c) four neat polymer films; (d) PBDTTT-*EE*:PCBM and PBDTTT-*DD*:PCBM 50% and 67% ratio BHJs. (e) Schematic representation of the polymer packing in BHJs from PBDTTT-*EE*:PCBM and PBDTTT-*DD*:PCBM.

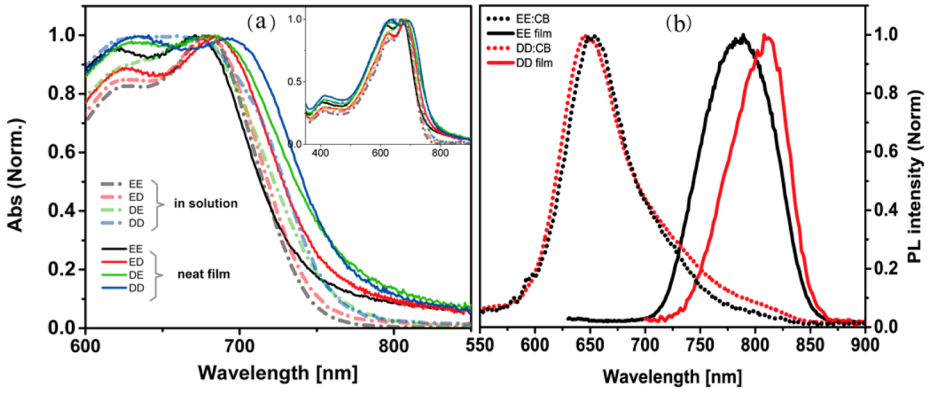

Figure 3. (a) Absorption spectra of four PBDTTT polymers in chlorobenzene solution (dash dot lines) and their neat films (solid lines) magnified in the 600−850 nm spectral range. Spectra are all normalized to the peak near 670 nm. Inset: normalized absorption spectra overlaid in the full 350−850 nm spectral region. (b) Normalized steady state PL spectra of two polymers, *EE* (black) and *DD* (red), measured in chlorobenzene solution (dots) and the neat films (solid lines).

shows that the scattering rings preserve their nonhomogenous intensity along in-plane direction for BHJs with polymers substituted with linear group such as *DD* and *DE* (Figure 2). This indicates the existence of polymer nanocrystallites in *DD* or *DE* even after blending with PCBM. On the contrary, for polymers with branched side chains such as *EE* and *ED*, the decreased order of crystalline polymer domains upon the mixing of PCBM indicates a good intercalation of PCBM molecules into the polymer chains. This is schematically shown in Figure 2e.

When comparing BHJs with different polymers (Figure 2d), we found a pronounced peak in line cut in the lower q region of <0.1 for *DD* due to scattering from nanocrystallites (the peak in the q > 0.1 region corresponding the d spacing of the polymer). For BHJ film with *EE*, contrary to *DD*, no obvious scattering peaks were observed for q < 0.1, which indicates no larger nanocrystallites present and further validates that the PCBM is intercalated well with the *EE* polymer. We extract average domain dimensions in the BHJ films by identifying the scattering peak and fitting the Guinier radius using Guinier's Law[61](details in the SI). The average domain radius in the 1:1 BHJs was determined to be *EE* ∼ 2.5 nm, *ED* ∼ 3 nm, *DE* 4.3-5 nm, and *DD* ∼ 6 nm assuming a spherical domain shape. The scattering peak intensity of 1:2 PBDTTT-*DD*:PCBM blend in

dx.doi.org/10.1021/ja503465s | J. Am. Chem. Soc. 2014, 136, 10024−10032

the lower q region of <0.1 is lower than that of 1:1 blend, indicating decrease in the nanocrystallite size when increasing the PCBM loading. Our AFM and GISAXS results presented here are in agreement with recent morphology characterization work on related PTB polymers.[10,46]

II.2. Interchain Interaction in Neat Polymer Films. The absorption features in solution phase (Figure 3) are similar for all four polymers with different side chains, confirming that the side chain substitution does not change electronic structure significantly for the isolated polymer chains. We model the solution phase absorption spectra of PBDTTT by TD-DFT calculations as shown in Figure S3 in the Supporting Information, which predict the S_0 to S_1 transition in good agreement with experimental results. The transition dipole of S_0 to S_1 (~670 nm) is along the direction of polymer conjugation (SI Figure S4).

Figure 3a illustrates absorption spectra from four neat polymers films normalized at the absorption peak near 670 nm. In the neat polymer films, the lowest absorption peak red-shifted to different extents compared to solution phase, from 5 nm for EE to 20 nm for *DD*. The red-shift in absorption peaks can be explained by interchain and intrachain interaction due to the aggregation of polymer chains.[30,62] In these polymer aggregates, planarization of the polymer backbone induced upon aggregation leads to red-shifting of optical transitions.[23,26,30,35,36] The oscillator strength of the low-energy aggregate absorption that extends beyond 800 nm is generally very weak because the transition is forbidden by symmetry.[26]

Significant red-shifted steady state photoluminescence (PL) peaks were also observed in neat polymer films compared to solution (Figure 3b), with *DD* having a more pronounced red shift compared with the *EE* (815 nm vs 780 nm, Figure 3b). The overall PL quantum yield of *DD* is lower, estimated to be ~50% of that of *EE*. We explain the red-shifted PL emission in the neat polymer films by exciton migration transferring the excitation to the lower energy emission sites.[24] Such sites are related to weakly emissive interchain species such as excimers and aggregates that are known to have lower energy than the intrachain excitons. The migration of energy to the lower energy sites is clearly demonstrated by global fit of time-resolved PL spectra as shown in Figure 4a. The PL decays are nonexponential with the high-energy side of the spectra having the shorter lifetime due to energy migration to lower energy sites. We attribute the red-shifted emission and lower quantum yield for the polymer with linear side chains such as *DD* to stronger interchain interaction in solid films.

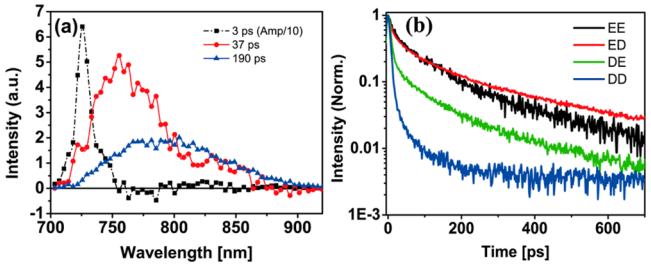

Figure 4. (a) Decay associated spectra of the PL decay of PBDTTT-*EE* pristine polymer film over a 700 ps time window. The 3 ps component is partially contributed by the excitation light scattering, and its amplitude is divided by 10. (b) Normalized, integrated PL decay from all four pristine polymer films based on the streak camera data. The PL intensities have been integrated over a 720–900 nm wavelength region.

II.3. Excited State Dynamics of Interchain and Intrachain Excitons. To further characterize the excited state dynamics of the intrachain and interchain states, we performed transient absorption measurements in neat films and 1:1 BHJs with PCBM (Figure 5). The pump wavelength was tuned to 665 nm to be resonant with the S_0–S_1 transition. In the transient absorption spectra of neat polymer films, all four polymers have similar spectral features. A very pronounced, broad excited state absorption (ESA) band centered at 1400 nm is observed shortly after photoexcitation for all four polymers. There is a smaller shoulder band near 1100 nm that becomes more prominent at later delay times.

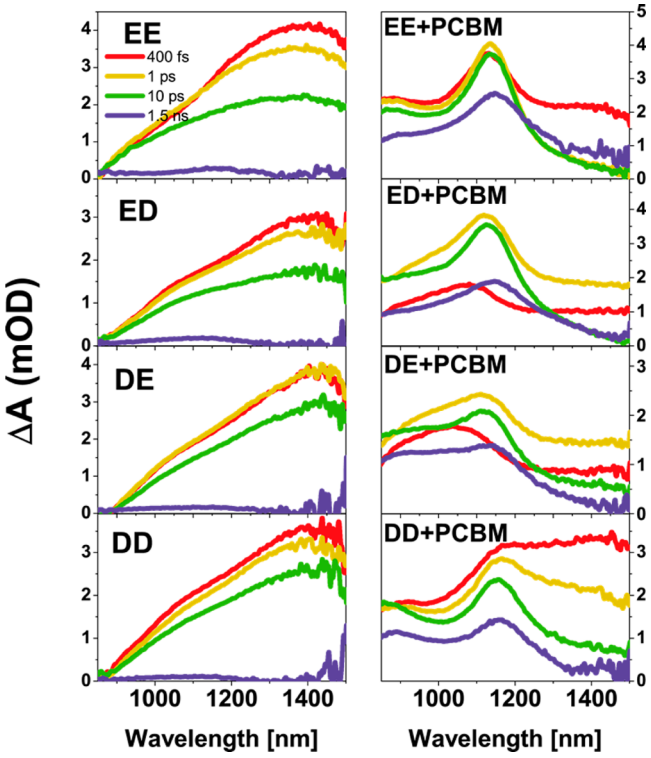

Figure 5. Transient absorption spectra acquired for four neat polymer films and their blends with PCBM (1:1 ratio) at different delays (400 fs, 1 ps, 10 ps, and 1.5 ns) after light excitation at 665 nm. The probe wavelength region spans from 850 to 1500 nm.

We compare the dynamics of the ESA band at 1400 nm to PL decay in neat polymer films in Figure 6. Figure 6a shows the PL decay traces for all neat polymer films measured at 750 nm with a 20 nm bandwidth using 670 nm excitation. *DD* has the fastest decay with an 11 ps lifetime followed by DE with a decay time of 17 ps. The decay in *EE* and *ED* is slowest, with decay lifetimes around 42 ps. A similar trend was observed when integrated over the whole PL spectra as shown previously in Figure 4b.

Most interestingly, excited state decay at 1400 nm deviated from the PL decay in neat polymer films to different extents depending on the side chain substitutions. We overlap PL decays with the transient absorption decay at 1400 nm in Figure 6b. Specifically, for the neat *EE* polymer film the PL and TA kinetic traces match very well after taking into account a slower instrument response in PL lifetime measurements, which indicates that the ESA at 1400 nm in the neat *EE* film is

dx.doi.org/10.1021/ja503465s | J. Am. Chem. Soc. 2014, 136, 10024–10032

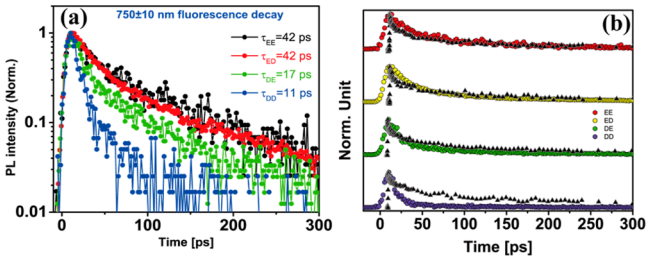

Figure 6. (a) Fluorescence decay of the neat polymer films centered at 750 nm (integrated with 20 nm bandwidth) after 670 nm light excitation, average life times are indicated in legends. (b) Comparing the fluorescence decay at 750 nm (circles) and the transient absorption measured at 1400 nm (black triangles).

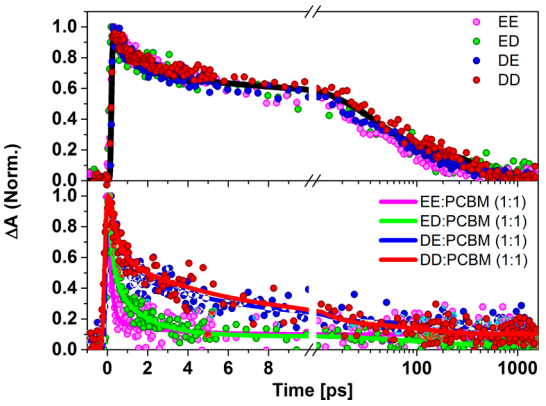

Figure 7. Exciton decay kinetics probed at 1500 nm over a 1.5 ns time window after 665 nm light excitation. The kinetics has been measured for all four polymers in both neat films and 1:1 BHJs (scattered points). Kinetic curves are fitted using up to three exponents (solid lines). All kinetic curves and their fitting results have been normalized to maxima. Note that the time axis is separated into two regimes: first 10 ps is in linear scale and the rest is shown in log scale for clarity.

due to emissive excitons. The deviation became more pronounced in polymers substituted with more linear side chains, with the largest difference between dynamics observed in the neat *DD* polymer film. Therefore, in the neat *DD* polymer film the ESA at 1400 nm no longer just reflects the states from which the PL originates.

We assign the broad 1400 nm band to overlapping absorption of intrachain excitons and interchain excitons. For the neat *EE* polymer film, the 1400 nm absorption has large contribution from bright intrachain excitons whereas dark interchain excitons dominate this absorption band in the neat *DD* film. Neat *DE* and *ED* films have contribution from both intrachain and interchain excitons. By tuning excitation wavelength to selectively excite lower energy interchain species, we again confirmed interchain excitons are the dominant species in neat *DD* film (for details, please see the text and Figure S10 in SI).

II.4. Molecular Packing Dependent Charge Separation Process in the BHJs. In this section we discuss charge separation pathways in BHJs proceeding from the morphology-related intrachain and interchain excitons. The right column of Figure 5 shows the TA spectra for BHJ films. The pump wavelength was tuned to 665 nm to be resonant with the lowest excitonic transition (S_0–S_1) to exclude charge separation from vibrationally hot excitons. For all BHJ films, the 1400 nm exciton absorption feature is significantly quenched, indicating that charge transfer to PCBM is possible from both the intrachain and interchain states.

As shown in Figure 5, the largely quenched 1400 nm band is replaced by a strong absorption band near 1130 nm. We assign the ∼1130 nm band to the cation absorption of the polymers due to charge separation between polymer donors and PCBM. To confirm this assignment, we performed steady state titration experiments by titrating the PBDTTT polymer with $FeCl_3$/chlorobenzene solution (Figure S5 in SI), and the 1130 nm absorption band indeed grows in with the addition of the oxidizing agent, which is consistent with previous work on related PTB polymers.[50]

We compare the ESA decay at 1400 nm in the four PCBM blended BHJ films in Figure 7. BHJ films with branched side chain substituted polymers lead to faster charge separation, with rates, summarized in SI Table T4, decreasing in the order of *EE* > *ED* > *DE* > *DD*. In the BHJs, the decay of the 1400 nm band ranging from ∼140 fs for *EE* to ∼5.3 ps for *DD*, considerably shorter than values of 30–80 ps observed in neat polymer films. The final charge separation yield in the BHJs was roughly estimated by taking the ground state bleaching (GSB) recovery at 650 nm on long time scale (1.5 ns), corresponding to free charges, divided by the maximum of the GSB signal (SI Figure S6). The lowest quantum yield was observed for the BHJ with *DD* (∼30%) while the highest (∼70%) is observed for the BHJ with *EE*. The kinetic curves and time constants for the fits are summarized in Table T4 in the SI.

To resolve the structure and associated lifetime of photoexcited species, we applied global analysis to obtain spectra of excited species and to estimate their lifetimes in the BHJ films.[63] The decay associated spectra (DAS) of excited state species with different lifetimes are given in Figure 8 (details are presented in the SI). The first DAS with the shortest lifetime (hundreds of fs) clearly revealed a positive feature of the ESA band (∼1400 nm) and a negative feature of the cation absorption band at ∼1130 nm, which reflects decay of the exciton absorption to form the polymer cation. For BHJs formed with *DE* and *DD* polymers, the second DAS also has a pronounced positive feature, but peaked at an even longer wavelength (>1400 nm), together with a negative dip around 1130 nm, indicating that a second and slower charge separation pathway on the order of a few ps exists in these BHJs. Note that in *EE*, this second pathway has little or no contribution, and the exciton absorption at 1400 nm is inevitably low because of the smaller exciton population, which leaves a purely negative dip in its DAS. The hundreds of picoseconds and nondecaying DAS are dominated by the decay of the polymer cation feature around 1130–1160 nm, which represents charge recombination.

We explain the morphology dependent charge separation pathways as follows. First we consider exciton diffusion limited pathways. The average domain radii as measured by GISAXS data are *EE* ∼ 2.5 nm, *ED* ∼ 3 nm, *DE* ∼ 4.3–5 nm, and *DD* ∼ 6 nm. Larger polymer crystallites in the BHJs of polymer with linear side chain substitution such as in *DE* and *DD* require a large fraction of excitons diffusing to the interface to be dissociated. Thus, the second and slower charge separation is at least partly due to time required for the exciton to diffuse to the interface. On the contrary, most excitons are created near a polymer/PCBM interface in the amorphous intercalation in *EE* BHJs. Recent work by Paraecatti et al. estimated that in another low-bandgap copolymer, PBDTTTPD, the spatial extent of its

dx.doi.org/10.1021/ja503465s | J. Am. Chem. Soc. 2014, 136, 10024–10032

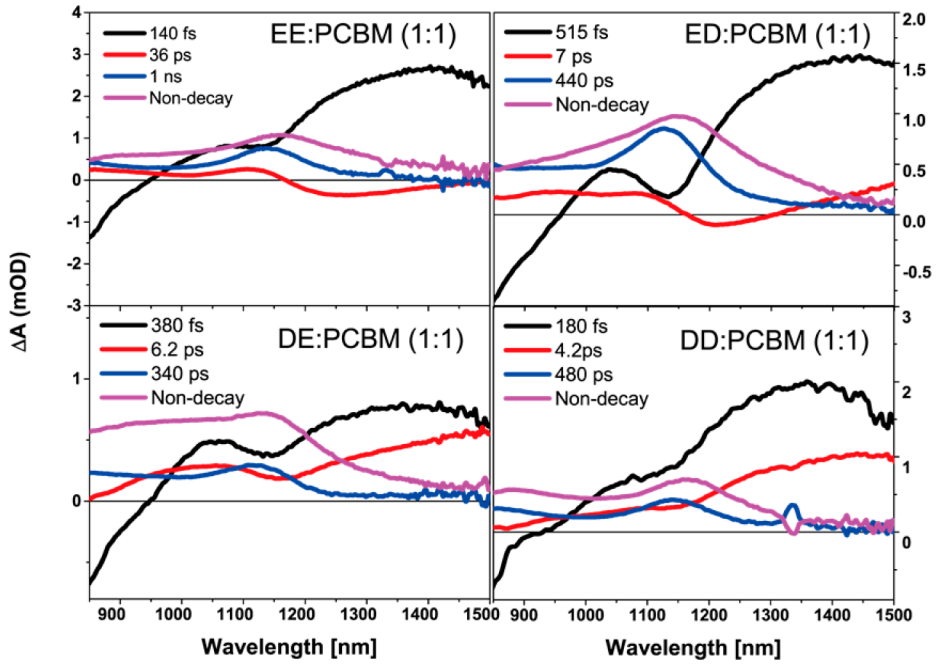

Figure 8. Decay-associated spectra from a global analysis of the transient absorption spectra gathered in four polymer−PCBM blended films. The probe wavelength region spans from 850 to 1500 nm. The spectra surfaces are fitted using three exponential decays plus a nondecay component.

exciton can be as large as 2 nm.[22] Because the domain size in EE is on the same order as the exciton size, no exciton diffusion is required. Therefore, direct charge separation pathway (<200 fs) dominates in *EE* BHJs.

We measure the exciton diffusion constant D in *EE* and *DD* neat films by performing pump intensity dependent PL lifetime measurements and assuming an exciton−exciton annihilation model following the methods described by Shaw et al.[64] (more details in the exciton diffusion section in SI). D is measured to be $(1.7 \pm 0.9) \times 10^{-2}$ cm^2 s^{-1} for *EE* and $(2.3 \pm 0.8) \times 10^{-1}$ cm^2 s^{-1} for *DD*. Assuming a one-dimensional diffusion, the diffusion length L is given by $L = (D\tau)^{1/2}$, where τ is the exciton lifetime. Using the exciton lifetime of 60 and 18 ps extracted from Figure 4b for *EE* and *DD*, respectively, L was found to be of 10 ± 3 nm and 19 ± 5 nm, respectively, for *EE* and *DD*. The more than 10-fold increase of D and almost 2-fold improvement of exciton diffusion length of *DD* compared to *EE* can be explained by the higher crystallinity. Exciton diffusion to 6 nm (average domain size given by GISAXS) in *DD* polymer domain will take ∼2 ps. This time is similar to but shorter than the second and slower charge separation time, which is ∼5 ps. This points toward other mechanisms possibly contributing to the slower charge separation pathway.

We further examine the effects of exciton diffusion by comparing charge separation dynamics of 1:1 and 1:3 *DD*:PCBM blends to those in the 1:1 blend (Figure 9). As shown in Figure 2d, the nanocrystalline size decreases with increased loading of PCBM as characterized by GISAXS. Interestingly, the charge separation dynamics of 1:1 and 1:3 DD:PCBM blends compared to the 1:1 blend are very similar even though the domain size is reduced in the 1:3 blend (Figure 9), again indicating there are other factors contributing to the slow charge separation pathway in addition to exciton diffusion.

Another possible contribution for a second and slower charge separation pathway on the order of a few ps for polymers with linear side chains is that interchain excitons have smaller driving

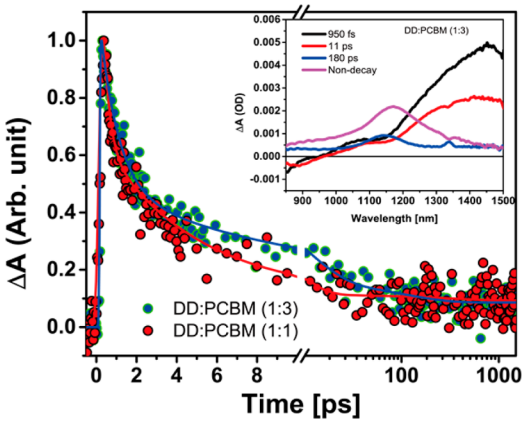

Figure 9. Exciton decay kinetics in *DD*:PCBM BHJs probed at 1400 nm over a 1.5 ns time window after 665 nm light excitation. Blue circles are measured in samples prepared with 1:3 volumetric ratio, and red circles are from 1:1 volumetric ratio ones. The fitting curve (solid line) is obtained from the global analysis results as shown in the inset. Inset: The decay associated spectra and the corresponding time constants resolved from a global analysis on the time-resolved spectra of the 1:3 *DD*:PCBM BHJs.

force available to overcome the Coulomb attraction. To gain a better understanding of morphology dependent energy levels of interchain states, quantum chemistry calculations have been performed. First, we investigate the possible formation of excimers by scanning the excited state potential energy surface along one internal coordinate: the distance between two face-to-face aromatic backbones of PBDTTT molecules (Figure 10a).

As the distance between two BDT-TT backbones increases, the potential energy of the excited state is not a monotonic function of the distance, but instead, a minimum point is found at a separation of around 3.7 Å indicating the presence of an excimer state (Figure 10a). When the distance between the two

dx.doi.org/10.1021/ja503465s | J. Am. Chem. Soc. 2014, 136, 10024−10032

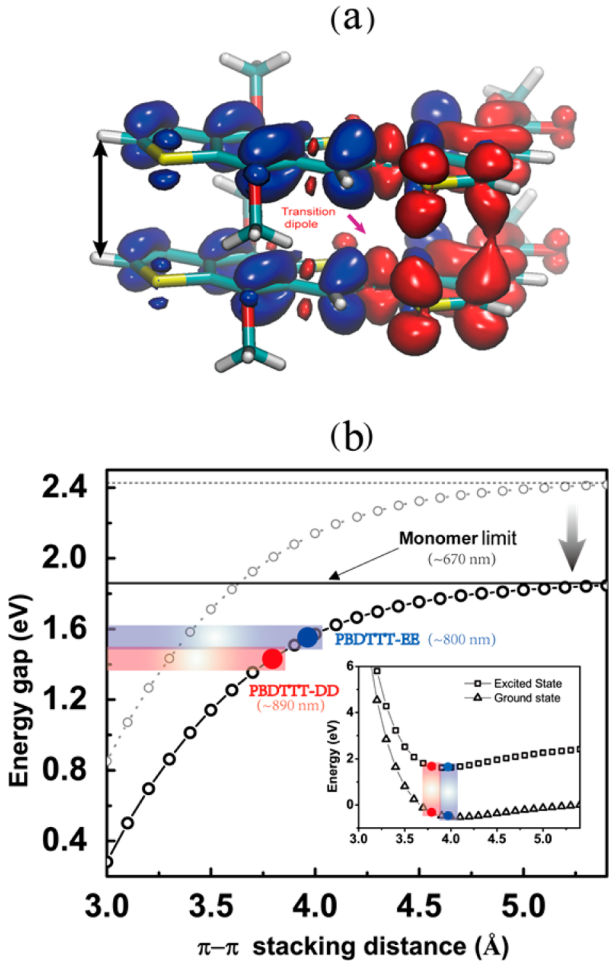

Figure 10. (a) PBDTTT dimer backbone being considered in the potential energy surface calculation; charge density difference between ground state and excited state are rendered in iso-value surfaces (red color represents electron density increase; blue represents electron density decrease, or holes). Red arrow indicates the orientation of the transition dipole of the lowest excited state (b) potential energy surface scan by varying the $\pi-\pi$ stacking distance using the method described in the text. The equilibrium point of the more tightly packed (PBDTTT-*DD*) and less tightly packed (PBDTTT-*EE*) polymers are indicated in red and blue, respectively. Note that the energies calculated are relative (gray open circles, limited by the conjugated length and calculation method), and the entire curve is shifted (black open circles) to match the isolated monomer limit measured in solution phase from experiment. Inset: the ground state and lowest excited state potential energy curve as a function of $\pi-\pi$ stacking distance.

chains increases, formation of an excimer is no longer preferred and the excited potential energy approaches the intrachain exciton energy.

The highly ordered *DD* polymer film has an interchain $\pi-\pi$ stacking distance of 3.7−3.8 Å (estimated from AFM imaging and GIWAXS pattern, Figures S5,S6, details in SI), which is very close to the lowest point of the lowest excited state potential curve (red dot in Figure 10b), resulting in stable formation of excimer. In contrast, in the more amorphous EE film this value is further away from the lowest point on the potential curve, and therefore does not have as stable an excimer state. We also point out here that the majority of the polymer chains in *EE* film are in an amorphous state, as its crystallinity is much lower than that of the *DD* polymer (6−7% crystallinity for EE and ∼30% for *DD*[59]). The lower excimer energy explains the preferential formation of excimers in the neat *DD* film over the *EE* film consistent with the PL and transient absorption results presented here.

Next, TD-DFT calculations were performed in three different PBDTTT molecular assemblies: a monolayer, a double layer, and a triple layer. Each layer is represented by a PBDTTT trimer backbone with a backbone plane spacing of 3.7 Å. Single point energy calculations were performed with TD-DFT at the wB97xd/6-31g(d) level. The bright transitions are colored black, and the dark transitions (oscillator strength <1% of the bright transitions) are colored gray in Figure 11.

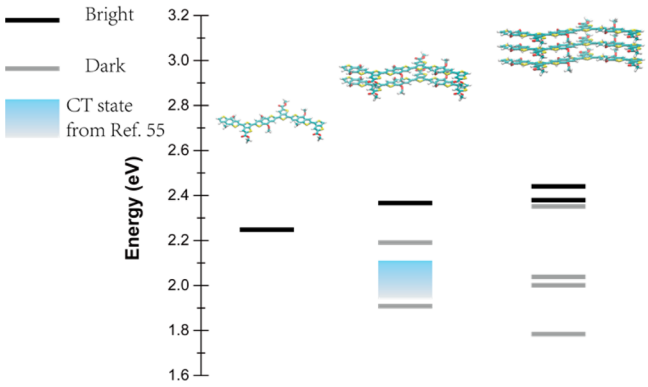

Figure 11. Energy level diagram of three PBDTTT molecular aggregates, from left to right: monolayer, double layer, and triple layer. The black lines represent the bright excited state transitions, while the gray lines represent the dark ones. By comparing the polymer energy levels in our work to the calculation in Borges et al.,[56] the relative position of the charge transfer (CT) states formed in the presence of PCBM is illustarated as the light blue region in the diagram.

As shown in Figure 11, the bright transitions in the interchain aggregates are higher in energy than the intrachain exciton at the single chain level—consistent with an H-aggregate model.[34] As the number of stacked layers grows, more interchain states are available due to the delocalization over multiple polymer backbones. Because most of the lower energy interchain states are dark, they potentially serve as traps of the bright excitons consistent with faster PL lifetime observed in *DD* (Figures 4 and 5).

A number of dark interchain exciton states are formed below the bright intrachain state and the charge transfer state to PCBM (Figure 11). We show the energetics of the charge transfer state as the blue bar in Figure 11. The driving force for exciton dissociation depends on the energy difference between the exciton and the charge transfer state. In recent work by Borges et al.,[56] an excess energy of 0.3 eV is available from the difference in energy between the vertical excitation to the bright intrachain $\pi-\pi^*$ state and the lowest charge transfer state. Many of the interchain exciton states have an excess energy of <0.3 eV for charge separation or even have a negative driving force that requires thermal activation. We conclude here that the higher probability of forming an excimer state as well as interchain states below the charge transfer state contribute partially to slower charge separation and even serve as traps for photoexcitation as observed in the transient absorption measurements.

In addition to exciton energy levels, the LUMO and HOMO levels and the energetics of the polarons also depend on the

dx.doi.org/10.1021/ja503465s | J. Am. Chem. Soc. 2014, 136, 10024−10032

molecular packing,[65] which can impact charge separation dynamics. For example, thermal annealing of P3HT has been found to raise the HOMO level (reduce ionizing potential) which in turn suppresses germinate recombination by stabilizing the charge separated state (lowering polaron energy).[65] To characterize the LUMO and HOMO level as a function of side chain functionality, we have performed cyclic voltammetry experiments to measure the LUMO and HOMO (details in the Supporting Information). HOMO and LUMO levels of different polymer films show a variation within 40 meV (Table T2 in the SI). Specifically, HOMO/LUMO is −5.15/−3.50 eV and −5.12/−3.53 eV, respectively, for *EE* and *DD*. We therefore conclude that the difference in driving force for exciton dissociation in this this group of polymers is contributed by the exciton energetics more significantly than by HOMO/LUMO levels.

Another important factor that determines device performance is charge recombination. From the DAS shown in Figure 8, PBDTTT-*EE*:PCBM BHJ not only has a larger amplitude in its nondecaying component than that in the PBDTTT-*DD*:PCBM BHJ (normalized to the total exciton amplitude at 1400−1500 nm in the two DAS, 50% vs 30%), but charge recombination in PBDTTT-EE:PCBM BHJs is also slower than in PBDTTT-*DD*:PCBM BHJs (1 ns vs 480 ps). This shows that recombination of free charges in BHJs based on *EE* is less likely than in those based on *DD*, *DE*, and *ED*. We conclude that efficient hole transport could be supported in the amorphous phase as indicated by the long-lived charge separated state in BHJ with EE polymers consistent with recent work of Noriega et al.[66]

III. CONCLUSION

Our results show that higher polymer crystallinity hinders charge separation in low bandgap copolymer blends. The reason for slower and less efficient charge separation is twofold: first, coarser phase segregation resulted from higher crystallinity polymer makes exciton diffusion a bottleneck for charge separation; and second, interchain excitons delocalized over multiple backbones that are more prevalent in the more crystalline polymer could lead to slower charge separation because they are energetically unfavorable for charge separation. Therefore, previous studies that suggest more delocalized interchain excitons in the polymer donor contribute to fast, sub-100 fs charge separation do not apply to the case of low band-gap copolymers.[8,17,21,46,67] An alternative mechanism for such ultrafast charge separation is provided by the high density of fullerene states energetically aligned with the donor exciton at the heterojunction.[16,18] In addition, unlike in homopolymers such as P3HT, where ordered lamellar layers formed by annealing can suppress the charge recombination in a device by enhancing hole transport and lowering polaron energies, the introduction of larger crystalline domains in PBDTTT polymers does not stabilize the charge separation; instead, faster charge recombination processes were observed. Both faster charge separation and slower recombination are the reasons the branched side chain substituted PBDTTT polymer devices have improved performance over the linear side chain modified ones.[46]

■ ASSOCIATED CONTENT

Supporting Information

Materials and methods include description of sample preparation, steady-state optical spectroscopy, PL lifetime measurements, femtosecond transient absorption spectroscopy, and DFT calculations. More details on AFM and GISAXS characterization of the BHJs, HOMO−LUMO gap calculation, cyclic voltammetry measurements, and steady state electrochemistry titration measurements are also presented. Summary of lifetime constants of kinetic decay, π-stacking distance characterization, excitation wavelength dependent transient absorbance spectra, and exciton diffusion measurements are also included. This material is available free of charge via the Internet at http://pubs.acs.org.

■ AUTHOR INFORMATION

Corresponding Author

*E-mail: lhuang2@nd.edu.

Notes

The authors declare no competing financial interest.

■ ACKNOWLEDGMENTS

Z. Guo and D. Lee acknowledge support from the Sustainable Energy Initiative of the University of Notre Dame. The authors thank the Center for Research Computing (CRC) at the University of Notre Dame for providing the computational resources for this work. The authors thank Dr. Ali Khounsary and Dr. Joseph Strzalka from Advanced Photon Sources at Argonne National Laboratory for performing the GIWAXS measurements. L. Huang was supported by the Division of Chemical Sciences, Geosciences and Biosciences, Office of Basic Energy Sciences of the U.S. Department of Energy through grant DE-FC02-04ER15533. Use of the Center for Nanoscale Materials was supported by the U.S. Department of Energy, Office of Science, Office of Basic Energy Sciences, under Contract No. DE-AC02-06CH11357. This publication is contribution No. NDRL 5019 from the Notre Dame Radiation Laboratory.

■ REFERENCES

(1) Clarke, T. M.; Durrant, J. R. *Chem. Rev.* **2010**, *110*, 6736.
(2) Yang, X.; Loos, J.; Veenstra, S. C.; Verhees, W. J. H.; Wienk, M. M.; Kroon, J. M.; Michels, M. A. J.; Janssen, R. A. J. *Nano Lett.* **2005**, *5*, 579.
(3) Mayer, A. C.; Scully, S. R.; Hardin, B. E.; Rowell, M. W.; McGehee, M. D. *Mater. Today* **2007**, *10*, 28.
(4) Coffey, D. C.; Reid, O. G.; Rodovsky, D. B.; Bartholomew, G. P.; Ginger, D. S. *Nano Lett.* **2007**, *7*, 738.
(5) Campoy-Quiles, M.; Campoy-Quiles, M.; Ferenczi, T.; Ferenczi, T.; Agostinelli, T.; Agostinelli, T.; Etchegoin, P. G.; Etchegoin, P. G.; Kim, Y.; Kim, Y.; Anthopoulos, T. D.; Anthopoulos, T. D.; Stavrinou, P. N.; Stavrinou, P. N.; Bradley, D. D. C.; Bradley, D. D. C.; Nelson, J.; Nelson, J. *Nat. Mater.* **2008**, *7*, 158.
(6) Chen, L. M.; Hong, Z. R.; Li, G.; Yang, Y. *Adv. Mater.* **2009**, *21*, 1434.
(7) Oosterhout, S. D.; Wienk, M. M.; van Bavel, S. S.; Thiedmann, R.; Koster, L. J. A.; Gilot, J.; Loos, J.; Schmidt, V.; Janssen, R. A. J. *Nat. Mater.* **2009**, *8*, 818.
(8) Marsh, R. A.; Hodgkiss, J. M.; Albert-Seifried, S.; Friend, R. H. *Nano Lett.* **2010**, *10*, 923.
(9) Howard, I. A.; Mauer, R.; Meister, M.; Laquai, F. *J. Am. Chem. Soc.* **2010**, *132*, 14866.
(10) Chen, W.; Xu, T.; He, F.; Wang, W.; Wang, C.; Strzalka, J.; Liu, Y.; Wen, J.; Miller, D. J.; Chen, J.; Hong, K.; Yu, L.; Darling, S. B. *Nano Lett.* **2011**, *11*, 3707.
(11) Schmidtke, J. P.; Friend, R. H.; Silva, C. *Phys. Rev. Lett.* **2008**, *100*, 157401.

(12) Huang, Y. S.; Westenhoff, S.; Avilov, I.; Sreearunothai, P.; Hodgkiss, J. M.; Deleener, C.; Friend, R. H.; Beljonne, D. *Nat. Mater.* **2008**, *7*, 483.
(13) Bakulin, A. A.; Dimitrov, S. D.; Rao, A.; Chow, P. C. Y.; Nielsen, C. B.; Schroeder, B. C.; McCulloch, I.; Bakker, H. J.; Durrant, J. R.; Friend, R. H. *J. Phys. Chem. Lett.* **2013**, *4*, 209.
(14) Dimitrov, S. D.; Bakulin, A. A.; Nielsen, C. B.; Schroeder, B. C.; Du, J.; Bronstein, H.; McCulloch, I.; Friend, R. H.; Durrant, J. R. *J. Am. Chem. Soc.* **2012**, *134*, 18189.
(15) Tamura, H.; Burghardt, I. *J. Am. Chem. Soc.* **2013**, *135*, 16364.
(16) Gélinas, S.; Rao, A.; Kumar, A.; Smith, S. L.; Chin, A. W.; Clark, J.; van der Poll, T. S.; Bazan, G. C.; Friend, R. H. *Science* **2014**, *343*, 512.
(17) Bittner, E. R.; Silva, C. *Nat. Commun.* **2014**, *5*, 3119.
(18) Savoie, B. M.; Rao, A.; Bakulin, A. A.; Gelinas, S.; Movaghar, B.; Friend, R. H.; Marks, T. J.; Ratner, M. A. *J. Am. Chem. Soc.* **2014**, *136*, 2876−2884.
(19) Bakulin, A. A.; Rao, A.; Pavelyev, V. G.; van Loosdrecht, P. H. M.; Pshenichnikov, M. S.; Niedzialek, D.; Cornil, J.; Beljonne, D.; Friend, R. H. *Science* **2012**, *335*, 1340.
(20) Tautz, R.; Da Como, E.; Wiebeler, C.; Soavi, G.; Dumsch, I.; Frohlich, N.; Grancini, G.; Allard, S.; Scherf, U.; Cerullo, G.; Schumacher, S.; Feldmann, J. *J. Am. Chem. Soc.* **2013**, *135*, 4282.
(21) Kaake, L. G.; Moses, D.; Heeger, A. J. *J. Phys. Chem. Lett.* **2013**, *4*, 2264.
(22) Paraecattil, A. A.; Banerji, N. *J. Am. Chem. Soc.* **2014**, *136*, 1472.
(23) Cornil, J.; dos Santos, D. A.; Crispin, X.; Silbey, R.; Brédas, J. L. *J. Am. Chem. Soc.* **1998**, *120*, 1289.
(24) Schwartz, B. J. *Annu. Rev. Phys. Chem.* **2003**, *54*, 141.
(25) Scholes, G. D.; Rumbles, G. *Nat. Mater.* **2006**, *5*, 683.
(26) Spano, F. C. *J. Chem. Phys.* **2005**, *122*, 234701.
(27) Scarongella, M.; Laktionov, A.; Rothlisberger, U.; Banerji, N. *J. Mater. Chem. C* **2013**, *1*, 2308.
(28) Yamagata, H.; Spano, F. C. *J. Phys. Chem. Lett.* **2014**, *5*, 622.
(29) Yan, M.; Rothberg, L.; Kwock, E.; Miller, T. *Phys. Rev. Lett.* **1995**, *75*, 1992.
(30) Nguyen, T.-Q.; Martini, I. B.; Liu, J.; Schwartz, B. J. *J. Phys. Chem. B* **2000**, *104*, 237.
(31) Österbacka, R.; An, C.; Jiang, X.; Vardeny, Z. *Science* **2000**, *287*, 839.
(32) Kim, J.; Swager, T. M. *Nature* **2001**, *411*, 1030.
(33) Reid, O. G.; Pensack, R. D.; Song, Y.; Scholes, G. D.; Rumbles, G. *Chem. Mater.* **2014**, *26*, 561.
(34) Spano, F. C.; Clark, J.; Silva, C.; Friend, R. H. *J. Chem. Phys.* **2009**, *130*, 074904.
(35) Beljonne, D.; Cornil, J.; Silbey, R.; Millie, P.; Bredas, J. L. *J. Chem. Phys.* **2000**, *112*, 4749.
(36) Habuchi, S.; Fujita, H.; Michinobu, T.; Vacha, M. *J. Phys. Chem. B* **2011**, *115*, 14404.
(37) Aryanpour, K.; Sheng, C.-X.; Olejnik, E.; Pandit, B.; Psiachos, D.; Mazumdar, S.; Vardeny, Z. V. *Phys. Rev. B* **2011**, *83*, 155124.
(38) Mukhopadhyay, S.; Jagtap, S. P.; Coropceanu, V.; Bredas, J. L.; Collard, D. M. *Angew. Chem., Int. Ed.* **2012**, *51*, 11629.
(39) Traub, M. C.; Vogelsang, J.; Plunkett, K. N.; Nuckolls, C.; Barbara, P. F.; Vanden Bout, D. A. *ACS Nano* **2012**, *6*, 523.
(40) Thiessen, A.; Vogelsang, J.; Adachi, T.; Steiner, F.; Vanden Bout, D.; Lupton, J. M. *Proc. Natl. Acad. Sci. U.S.A.* **2013**, *110*, E3550.
(41) Brown, P. J.; Thomas, D. S.; Köhler, A.; Wilson, J. S.; Kim, J.-S.; Ramsdale, C. M.; Sirringhaus, H.; Friend, R. H. *Phys. Rev. B* **2003**, *67*, 064203.
(42) Yu, J.; Hu, D.; Barbara, P. F. *Science* **2000**, *289*, 1327.
(43) Schaller, R. D.; Lee, L. F.; Johnson, J. C.; Haber, L. H.; Saykally, R. J.; Vieceli, J.; Benjamin, I.; Nguyen, T.-Q.; Schwartz, B. J. *J. Phys. Chem. B* **2002**, *106*, 9496.
(44) Kohler, A.; Hoffmann, S. T.; Bassler, H. *J. Am. Chem. Soc.* **2012**, *134*, 11594.
(45) Park, S. H.; Roy, A.; Beaupré, S.; Cho, S.; Coates, N.; Moon, J. S.; Moses, D.; Leclerc, M.; Lee, K.; Heeger, A. J. *Nat. Photonics* **2009**, *3*, 297.
(46) Szarko, J. M.; Guo, J.; Liang, Y.; Lee, B.; Rolczynski, B. S.; Strzalka, J.; Xu, T.; Loser, S.; Marks, T. J.; Yu, L.; Chen, L. X. *Adv. Mater.* **2010**, *22*, 5468.
(47) Li, G.; Zhu, R.; Yang, Y. *Nat. Photonics* **2012**, *6*, 153.
(48) Guo, X. G.; Zhou, N. J.; Lou, S. J.; Smith, J.; Tice, D. B.; Hennek, J. W.; Ortiz, R. P.; Navarrete, J. T. L.; Li, S. Y.; Strzalka, J.; Chen, L. X.; Chang, R. P. H.; Facchetti, A.; Marks, T. J. *Nat. Photonics* **2013**, *7*, 825.
(49) Lu, L.; Yu, L. *Adv. Mater.* **2014**, DOI: 10.1002/adma.201400384.
(50) Rolczynski, B. S.; Szarko, J. M.; Son, H. J.; Liang, Y.; Yu, L.; Chen, L. X. *J. Am. Chem. Soc.* **2012**, *134*, 4142.
(51) Szarko, J. M.; Rolczynski, B. S.; Lou, S. J.; Xu, T.; Strzalka, J.; Marks, T. J.; Yu, L.; Chen, L. X. *Adv. Funct. Mater.* **2014**, *24*, 10.
(52) Tautz, R.; Da Como, E.; Limmer, T.; Feldmann, J.; Egelhaaf, H. J.; von Hauff, E.; Lemaur, V.; Beljonne, D.; Yilmaz, S.; Dumsch, I.; Allard, S.; Scherf, U. *Nat. Commun.* **2012**, *3*, 970.
(53) Banerji, N. *J. Mater. Chem. C* **2013**, *1*, 3052.
(54) Hwang, I.; Beaupré, S.; Leclerc, M.; Scholes, G. D. *Chem. Sci.* **2012**, *3*, 2270.
(55) Huang, Y.-S.; Gierschner, J.; Schmidtke, J. P.; Friend, R. H.; Beljonne, D. *Phys. Rev. B* **2011**, *84*, 205311.
(56) Borges, I., Jr.; Aquino, A. J.; Kohn, A.; Nieman, R.; Hase, W. L.; Chen, L. X.; Lischka, H. *J. Am. Chem. Soc.* **2013**, *135*, 18252−18255.
(57) Kim, Y.; Cook, S.; Tuladhar, S.; Choulis, S.; Nelson, J.; Durrant, J.; Bradley, D.; Giles, M.; McCulloch, I.; Ha, C.; Ree, M. *Nat. Mater.* **2006**, *5*, 197.
(58) Mei, J.; Bao, Z. *Chem. Mater.* **2014**, *26*, 604.
(59) Guo, Z.; Lee, D. Y.; Liu, Y.; Sun, F. Y.; Sliwinski, A.; Gao, H. F.; Burns, P. C.; Huang, L. B.; Luo, T. F. *Phys. Chem. Chem. Phys.* **2014**, *16*, 7764.
(60) Hou, J.; Chen, H.-Y.; Zhang, S.; Chen, R. I.; Yang, Y.; Wu, Y.; Li, G. *J. Am. Chem. Soc.* **2009**, *131*, 15586.
(61) Guinier, A.; Fournet, G.; Walker, C. B.; Yudowitch, K. L. *Small-angle scattering of X-rays*; Wiley: New York, 1955; Vol. *14*.
(62) Jiang, X. M.; Osterbacka, R.; Korovyanko, O.; An, C. P.; Horovitz, B.; Janssen, R. A. J.; Vardeny, Z. V. *Adv. Funct. Mater.* **2002**, *12*, 587.
(63) van Stokkum, I. H. M.; Larsen, D. S.; Van Grondelle, R. *Biochim. Biophys. Acta* **2004**, *1657*, 82.
(64) Shaw, P. E.; Ruseckas, A.; Samuel, I. D. W. *Adv. Mater.* **2008**, *20*, 3516.
(65) Clarke, T. M.; Ballantyne, A. M.; Nelson, J.; Bradley, D. D. C.; Durrant, J. R. *Adv. Funct. Mater.* **2008**, *18*, 4029.
(66) Noriega, R.; Rivnay, J.; Vandewal, K.; Koch, F. P. V.; Stingelin, N.; Smith, P.; Toney, M. F.; Salleo, A. *Nat. Mater.* **2013**, *12*, 1038.
(67) Chen, K.; Barker, A. J.; Reish, M. E.; Gordon, K. C.; Hodgkiss, J. M. *J. Am. Chem. Soc.* **2013**, *135*, 18502.